


Article

Corrosion Behavior of Si Diffusion Coating on an Austenitic Fe-Base Alloy in High Temperature Supercritical-Carbon Dioxide and Steam Environment

Sung Hwan Kim, Chaewon Kim, Ji-Hwan Cha and Changheui Jang * 

Department of Nuclear and Quantum Engineering, Korea Advanced Institute of Science and Technology, Daejeon 34141, Korea; sciencetom@kaist.ac.kr (S.H.K.); kcw9591@kaist.ac.kr (C.K.); jh_cha@kaist.ac.kr (J.-H.C.)

* Correspondence: chjang@kaist.ac.kr

Received: 27 April 2020; Accepted: 19 May 2020; Published: 21 May 2020



Abstract: In order to enhance corrosion resistance of stainless steel (SS) 316LN at high temperature environments, surface modification was carried out by Si deposition and subsequent heat treatment at 900 °C for 1 h. This resulted in the formation of $\text{Fe}_5\text{Ni}_3\text{Si}_2$ phase on the surface region. The surface-modified alloy was exposed to high temperature S- CO_2 (650 °C, 20 MPa) and steam (650 °C, 0.1 MPa) for 500 h and evaluated for its corrosion behavior in comparison to the as-received alloy. In S- CO_2 environment, the as-received SS 316LN showed severe oxide spallation and thick Fe-rich oxide formation, while the surface-modified alloy formed a continuous and adherent Si- and Cr-rich oxide layer. In steam, as-received SS 316LN formed very thick duplex Fe- and Cr-rich oxide layers. On the other hand, surface-modified SS 316LN formed notably thinner oxides, which could be attributed to the formation of Si-rich oxide under outer Fe-rich oxides on the surface-modified alloy. Thus, in view of the weight changes, oxide thickness, and morphologies of the two conditions, it was found that Si diffusion coating was effective in improving the corrosion resistance of SS 316LN in both S- CO_2 and steam environments.

Keywords: silicide diffusion coating; austenitic alloy; corrosion; supercritical-carbon dioxide; high temperature steam

1. Introduction

With increasing operating temperatures of next generation power plants for greater efficiency, Ni-base alloys with high creep and corrosion resistance are likely to be used for critical load-bearing components such as turbine blades. On the other hand, it would be more economically practical to use less costly Fe-base alloys for other components that are subjected to lower levels of load. Fe-base alloys generally exhibit lower corrosion resistances than Ni-base alloys in high temperature environments above 600 °C. For example, it has been reported that stainless steel (SS) 316LN showed significantly higher weight gains compared to other alloys after exposure to supercritical-carbon dioxide (S- CO_2) at 650 °C (20 MPa) for up to 3000 h [1]. This was due to spallation of initially formed continuous Cr-rich oxide layer followed by growth of thick Fe-rich oxides. Similarly, severe oxide spallation was reported for SS 316L when exposed in steam at 650 °C (0.1 MPa) for up to 5000 h [2].

In this regard, surface modification may be applied to improve corrosion resistance of such alloys. Si is known to be beneficial in terms of oxidation resistance by formation of SiO_2 layer at the oxide/metal interface. Nguyen et al. conducted corrosion tests of Fe-base model alloys with different Si contents in CO_2 at 650 °C and reported significantly lower weight gains with greater Si contents [3]. Moon et al. reported high oxidation resistance of a Fe-20Cr-2Si alloy even in steam environment at 1200 °C [4]. These behaviors were attributed to the formation of a continuous amorphous SiO_2 layer

at the metal/oxide interface. Meanwhile, studies on applications of Si coatings on Fe-base alloys and evaluations of high temperature corrosion behavior are rather scarce.

In this study, Si coating and heat treatment was employed to form a Si-rich layer on an austenitic Fe-base alloy, SS 316LN. Then, the surface-modified alloy was subjected to corrosion tests in high temperature S-CO₂ (650 °C, 20 MPa) and steam (650 °C, 0.1 MPa) environments for 500 h. The corrosion behavior of the surface-modified alloy was evaluated and discussed in comparison to those of the as-received SS 316LN.

2. Materials and Methods

2.1. Test Materials and Surface Modification Procedure

The chemical composition of SS 316LN used in this study was analyzed by inductively coupled plasma (ICP) spectroscopy and listed in Table 1. The material was machined into coupon-type specimens (12 mm in diameter, 1 mm thickness and 1.5 mm diameter hole for hanging during corrosion tests) by electro-discharge machining (EDM). The specimens were mechanically ground up to 1200 grit using SiC emery papers and ultra-sonically cleaned in ethanol prior to either surface modification or corrosion test.

Direct current (DC) magnetron sputtering was used to deposit a Si layer on the coupon specimens. The coating procedure is similar to a previous study by the authors [5]. First, the specimens were placed in the coating chamber, after which the chamber was pumped to reach high vacuum state ($\leq 3.0 \times 10^{-6}$ Torr). Then, magnetron sputtering was conducted under the conditions listed in Table 2, resulting in a 1.8 μm thick Si layer on the specimens. Subsequently, the specimens were flipped and the procedure was repeated to coat both sides of the specimens. The Si-coated specimens were subjected to inter-diffusion heat treatment (IDHT) at 900 °C for 1 h to form a silicide diffusion coating layer, so that coating/matrix adhesion would be improved. IDHT was conducted in a high vacuum environment ($\leq 3.0 \times 10^{-6}$ Torr) in order to avoid unintended oxidation prior to exposure in high temperature S-CO₂ and steam environments.

Table 1. Chemical compositions of SS 316LN used in this study analyzed by inductively coupled plasma (ICP) (in wt.%).

Alloy	Fe	Cr	Ni	Mo	Mn	Si	C	N
SS 316LN	Bal.	18.9	13.9	2.78	1.93	0.63	0.03	0.16

Table 2. Working conditions of magnetron sputtering used in this study.

Target	Base Pressure	Working Gas	Working Pressure	Power	Duration
Si (99.99% purity)	$\leq 3.0 \times 10^{-6}$ Torr	Ar (99.999% purity)	0.003 Torr	DC 100 W (1 gun)	4 h

2.2. High Temperature Corrosion Tests

Corrosion tests were conducted in S-CO₂ environment at 650 °C (20 MPa) and steam environment at 650 °C (0.1 MPa) for 500 h. Two coupon specimens of each condition (as-received and surface-modified) were exposed to each corrosion test environment. For S-CO₂ corrosion test, the specimens were installed in the S-CO₂ autoclave, which was then sealed. Then, the autoclave was heated to the target temperature of 650 °C, while research-grade CO₂ (99.999% purity) was pumped into the autoclave. The internal pressure of the autoclave was maintained at 20 MPa by a back pressure regulator (BPR) installed at the gas outlet. After the test duration reached 500 h, the heaters were turned off and the autoclave was left to cool to room temperature. The details of the test equipment and procedure for S-CO₂ corrosion test were described in the previous study [6].

The steam corrosion test system consisted of a water pump, a preheater, and test chamber. After the specimens were installed in the test chamber, the preheater and test chamber were heated at a rate of 5 °C/min to target temperatures of 500 and 650 °C, respectively. Then, deaerated distilled water with dissolved oxygen content of less than 150 ppb was pumped into the system at a rate of 20 cc/min. The water turned to steam as it passed through the preheater, and was introduced into the test chamber. After 500 h of steam corrosion test, the heaters and pump were turned off and the specimens were left to cool to room temperature. Further description of the steam corrosion test equipment can be found in the previous study [7].

Weight changes of the specimens after corrosion tests were measured using an electronic microbalance (Mettler Toledo AT21 Comparator, Mettler Toledo Inc., Columbus, OH, USA) with a resolution of 0.001 mg. For oxide and microstructure analyses, X-ray diffraction (XRD, Rigaku D/MAX-2500, Rigaku Co., Tokyo, Japan), scanning electron microscopy (SEM, FEI Magellan400, FEI Co., Hillsboro, OR, USA) equipped with energy dispersive X-ray spectroscopy (EDS) and transmission electron microscopy (TEM, FEI Talos F200X, Thermo Fisher Scientific Inc., Waltham, MA, USA) equipped with EDS was used. SEM was used at an accelerating voltage of 10 kV and current of 0.8 nA, while TEM was operated at accelerating voltage of 200 kV and current of 1 nA. TEM specimens were fabricated using focused ion beam (FIB, Helios Nanolab 450 F1, FEI Co., Hillsboro, OR, USA).

3. Results and Discussion

3.1. Characterization of the Surface-Modified Region

Figure 1 shows the results of XRD analysis on SS 316LN after Si deposition and IDHT (900 °C, 1 h). Other than the peaks from the matrix, peaks of $\text{Fe}_5\text{Ni}_3\text{Si}_2$ silicide phase were detected. Surface SEM micrograph shows that a continuous surface layer with somewhat blocky morphology was formed (Figure 2a). Cross-sectional backscattered electron (BSE) micrograph of the specimen is shown in Figure 2b. A surface layer with different contrast from the adjacent matrix can be identified. This region would correspond to $\text{Fe}_5\text{Ni}_3\text{Si}_2$ silicide phase detected by XRD analysis. Figure 2c shows the result of EDS line scanning along the dotted arrow indicated in the BSE micrograph. The surface region is enriched in Si about 10 wt.% and about 9 μm in thickness. In addition, Fe, Ni, and Cr contents in this layer are about 45, 18, and 14 wt.%, respectively. This indicates that interdiffusion of the deposited Si layer and elements in the matrix occurred during heat treatment at 900 °C, and formed $\text{Fe}_5\text{Ni}_3\text{Si}_2$ phase. Previously, Zhang et al. evaluated the phase equilibria of Fe-Ni-Si system at 850 °C and confirmed $\text{Fe}_5\text{Ni}_3\text{Si}_2$ phase as thermodynamically stable phase in Fe and Ni composition ranges of 46.5–56.3 at.% and 23.6–32.5 at.%, respectively [8].

Meanwhile, discontinuous voids were observed in the Si-enriched layer. High C region in EDS line scan result (Figure 2c) corresponds to the void, as the voids were filled by C-rich resin during sample mounting for cross-sectional analyses. These voids would have formed during heat treatment due to faster outward diffusion of matrix elements toward the Si coating layer. Perez et al. also reported formation of voids on Si diffusion-coated SS 304 at the coating/alloy interface [9]. Such Kirkendall voids may be avoided by optimization of heat treatment temperature. On the other hand, relative enrichment of Mo was noted adjacent to the voids (Figure 2c). The change in chemical compositions due to Si-enrichment at the surface during heat treatment would result in activity changes, which in turn would have resulted in Mo diffusion from the underlying matrix toward the coating/matrix interface. This is indicated by depletion of Mo below the region of Mo-enrichment shown in EDS line scan result (Figure 2c).

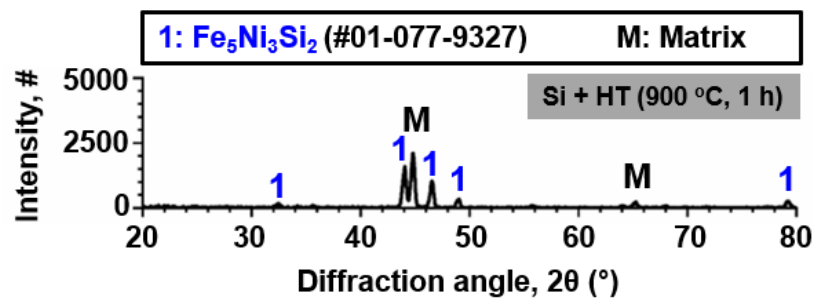


Figure 1. Result of X-ray diffraction (XRD) analysis conducted on the surface-modified (Si-coated and heat-treated) SS 316LN.

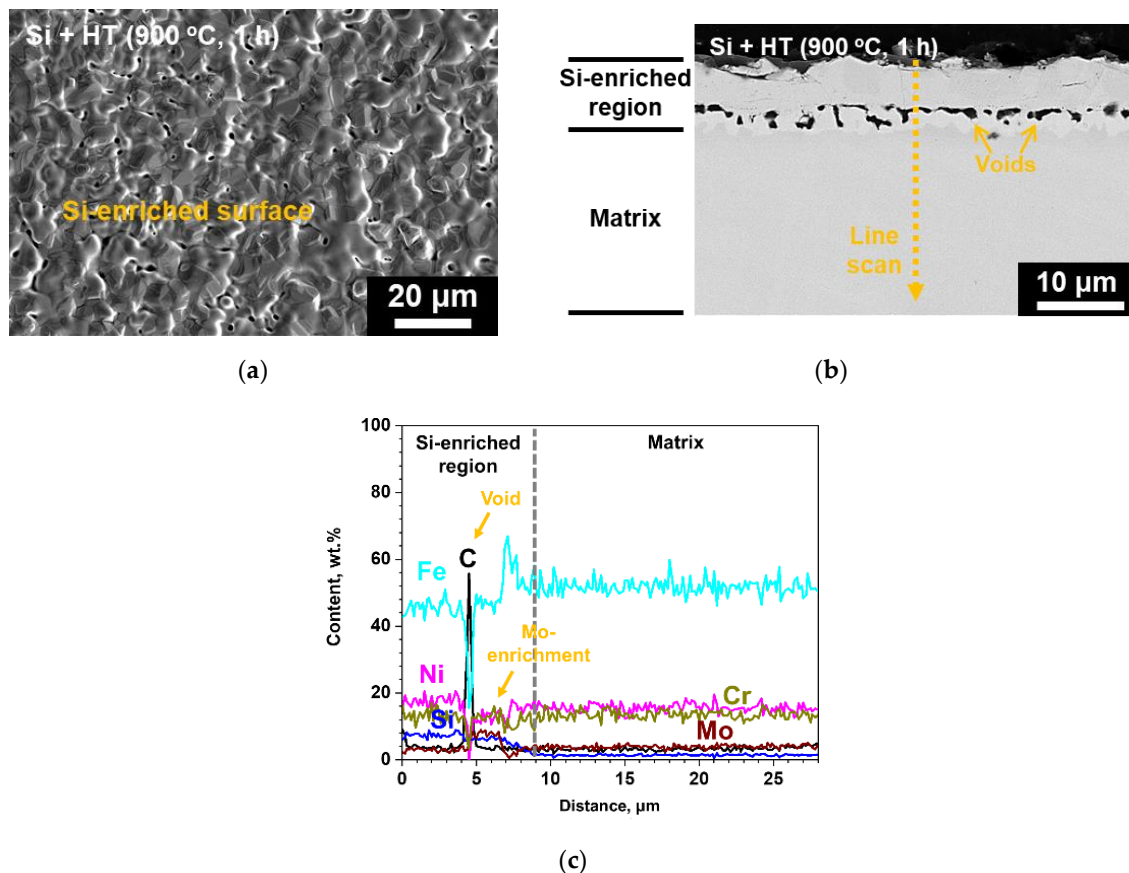


Figure 2. (a) Surface scanning electron microscopy (SEM), (b) cross-sectional backscattered electron (BSE) micrograph of the surface-modified SS 316LN, and (c) result of energy dispersive X-ray spectroscopy (EDS) line scan along the dotted line in (c).

3.2. Weight Changes after Corrosion Tests in S-CO₂ and Steam

Weight changes of the as-received and surface-modified SS 316LN after exposure to S-CO₂ (650 °C, 20 MPa, 500 h) and steam (650 °C, 0.1 MPa, 500 h) environments are shown in Figure 3. The average weight change values of the two specimens of each condition are also listed in the figure. As shown in the figure, weight gain in S-CO₂ environment is lower for the as-received condition than that of the surface-modified specimen. However, it should be mentioned that reported weight change values of the as-received SS 316LN can vary in high temperature S-CO₂ environments under same conditions due to oxide spallation. For example, in a previous study, it was reported that the as-received SS 316LN showed weight gain of 0.44 mg/cm² after exposure to S-CO₂ at 650 °C (20 MPa) for 500 h [5]. Still, another study reported weight gain of about 0.1 mg/cm² for the as-received SS 316LN corroded in the same condition [10].

In this study, the as-received SS 316LN had weight gain of 0.099 mg/cm^2 . Such discrepancies in weight change values of as-received SS 316LN tested in similar conditions can be ascribed to different times at which oxide spallation and subsequent Fe-rich oxide formation occurs on 316LN in high temperature environments above 600°C . In this regard, the small variance between the weight change values of the two as-received samples in this study would be coincidental. To the contrary, as will be shown in the next section, oxide spallation was not observed for the surface-modified SS 316LN after S-CO₂ exposure. Thus, the weight change comparisons between the as-received and surface-modified conditions after S-CO₂ corrosion may not be an accurate representation of the actual corrosion resistances.

In the case of specimens exposed to steam environment, weight gains of the surface-modified specimen is about half that of the as-received specimen. It is notable that weight gains are significantly greater for steam-exposed specimens compared to those exposed to S-CO₂. It has been reported that high pressure of S-CO₂ results in greater corrosion rates compared to atmospheric pressure CO₂ [11]. However, even with higher pressure of S-CO₂ of 20 MPa, steam at atmospheric pressure resulted in greater oxidation. It has been suggested that hydrogen would be generated by oxidation in steam [12]. The hydrogen as proton ions would permeate into the oxide and change its structure and oxidation behavior. Kim et al. compared the corrosion characteristics of Ni-base alloys in steam at 900°C with and without hydrogen addition, and found that corrosion rates were greater in hydrogen-added steam [7]. On the other hand, hydrogen would not be produced in S-CO₂ environment, which may be a factor in lower weight gains in S-CO₂ compared to that in steam.

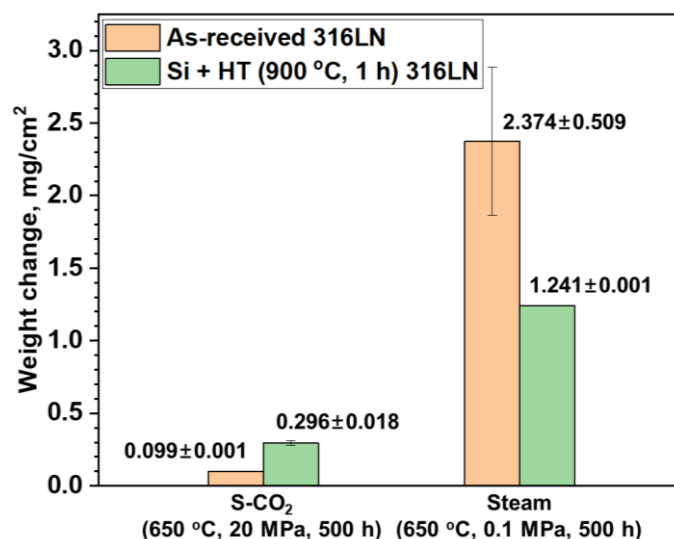


Figure 3. Weight changes of the as-received and surface-modified SS 316LN after exposure to S-CO₂ (650 °C, 20 MPa, 500 h) and steam (650 °C, 0.1 MPa, 500 h) environments.

3.3. Characterization of Oxides Formed in High Temperature S-CO₂

Figure 4 shows the results of XRD analysis of the as-received and surface-modified SS 316LN after exposure in S-CO₂ at 650°C (20 MPa) for 500 h. For the as-received SS 316LN, peaks of chromia (Cr₂O₃) and Fe-rich oxides (mainly Fe₂O₃) were found. For the surface-modified specimen, chromia peaks were detected, along with peaks of Fe₅Ni₃Si₂ phase and matrix that were observed before corrosion test (Figure 1). Figure 5a shows the plan-view SEM micrograph of the oxides formed on the as-received SS 316LN after S-CO₂ exposure. Severe spallation of a thin oxide layer and formation of thick oxides can be noted. EDS analysis (not shown) confirmed that the thin oxide layer was mainly rich in Cr while the thick oxide was rich in Fe, which is in agreement with previous studies [1,2]. Cross-sectional backscattered electron (BSE) micrograph of this specimen is shown in Figure 5b. The Cr-rich oxide layer was difficult to find due to spallation, while thick Fe-rich oxide region was seen. EDS line scan results indicated that this oxide was about $5 \mu\text{m}$ in thickness, while it consisted of a duplex structure

with outer oxide being Fe-rich and inner oxide being rich in both Fe and Cr (Figure 5c). Such oxides would have formed because of depletion of Cr in the underlying matrix after oxide spallation.

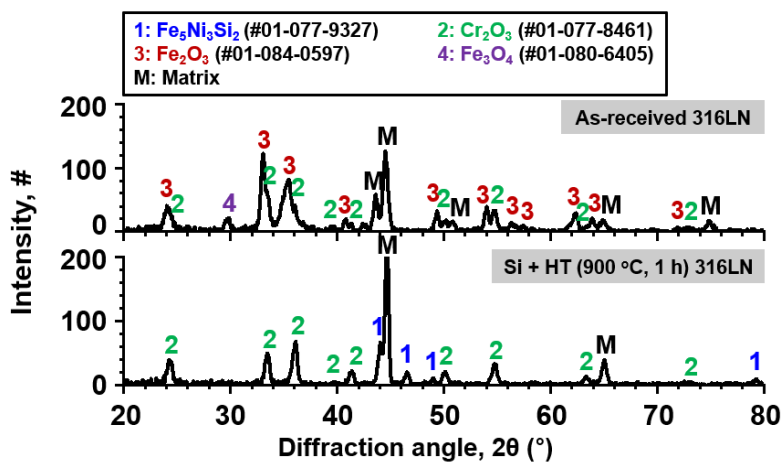


Figure 4. Result of XRD analysis conducted on the as-received and surface-modified SS 316LN after exposure to S-CO₂ at 650 °C (20 MPa) for 500 h.

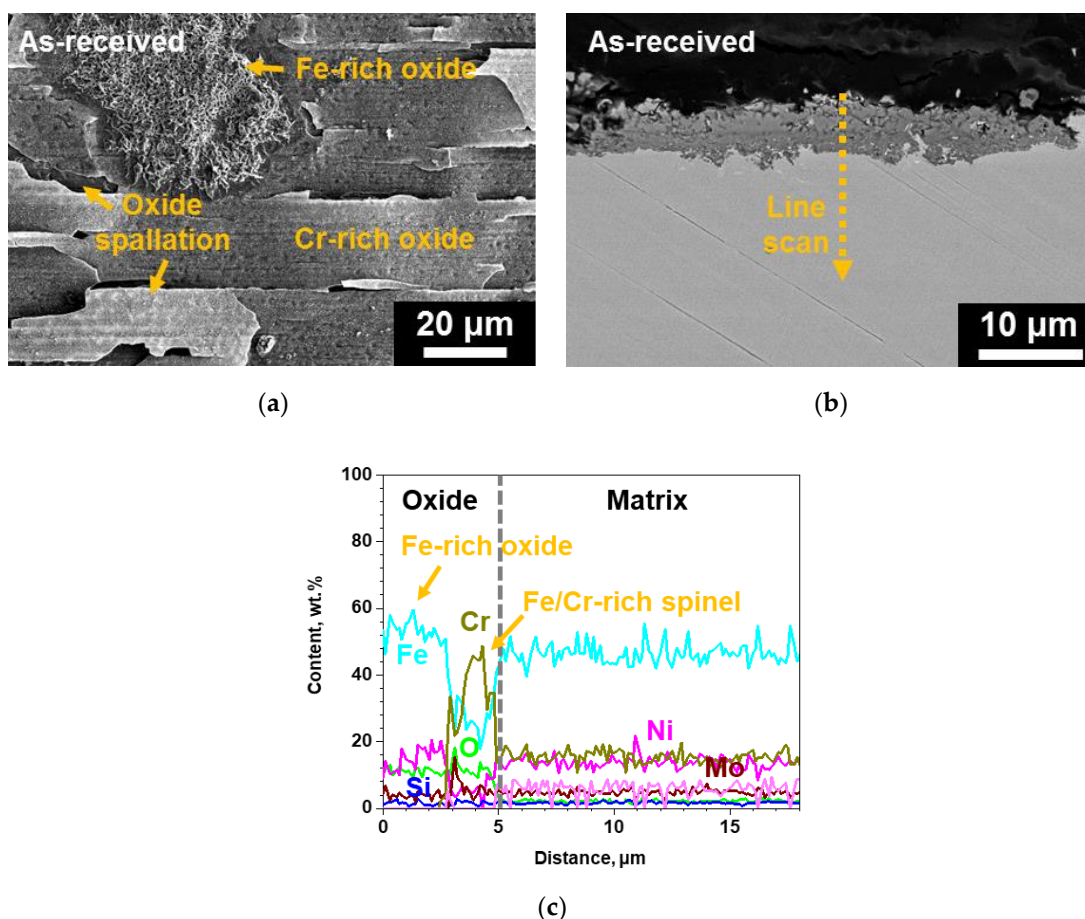


Figure 5. (a) Surface SEM, (b) cross-sectional BSE micrograph of the as-received SS 316LN after exposure to S-CO₂ at 650 °C (20 MPa) for 500 h, and (c) result of EDS line scan along the dotted line in (b).

In the case of the surface-modified specimen, a continuous oxide could be observed in the surface SEM micrograph, while oxide spallation was not observed (Figure 6a). In addition, the oxides have a blocky and nodular morphology, similar to that of the surface of the surface-modified specimen

before corrosion test shown in Figure 2a. This suggests that the oxide formed on the surface-modified specimen is rather thin. From cross-sectional BSE micrograph and EDS line scanning (Figure 6b,c), it was observed that the oxide had a thickness of about 2 μm and was rich mainly in Cr and Si. Thus, from the thin adherent oxide formed on the surface-modified SS 316LN in contrast to spalled Cr-rich oxides and locally thick Fe-rich oxides formed on the as-received SS 316LN, it is quite clear that corrosion resistance of the surface-modified SS 316LN is better than the as-received SS 316LN in S-CO₂.

TEM analyses results of the oxide layer formed on the surface-modified specimen after S-CO₂ exposure are shown in Figure 7. The oxide is mainly rich in Si, while some discontinuous Cr-rich oxides can also be observed. It is interesting to note that Si-rich oxides were not observed in XRD analysis results, while only chromia peaks were found (Figure 4). This would be due to the amorphous nature of the Si-rich oxide, so that diffraction peaks could not be detected by XRD. SiO₂ is reported to be typically amorphous under 1000 °C [13], and its formation has been reported for various Si-containing alloys at the oxide/matrix interface after exposure to high temperatures oxidizing environments [3,14,15]. Meanwhile, one of the voids that was observed in the Si-enriched region of surface-modified alloy (Figure 2) after S-CO₂ exposure can be seen in Figure 7a. Oxidation occurred around the voids, and the formed oxides were mainly Si-rich.

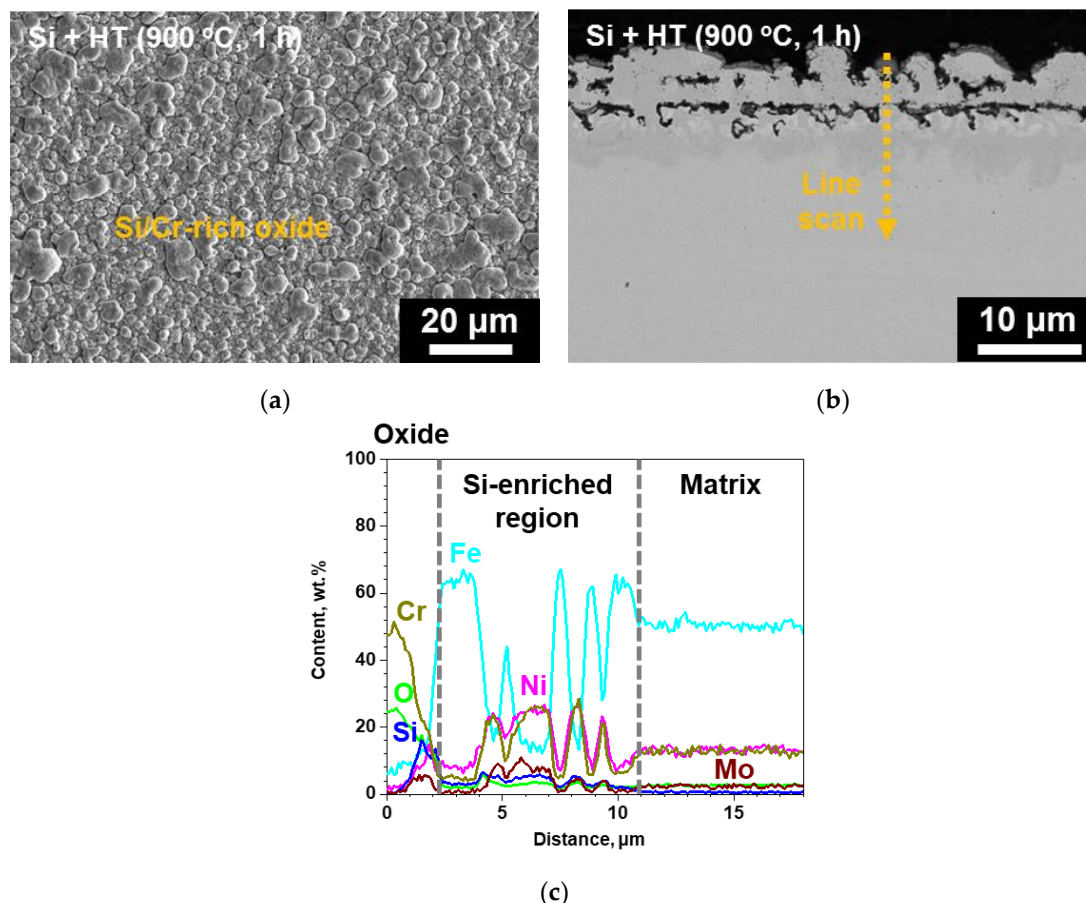


Figure 6. (a) Surface SEM, (b) cross-sectional BSE micrograph of the surface-modified SS 316LN after exposure to S-CO₂ at 650 °C (20 MPa) for 500 h, and (c) result of EDS line scan along the dotted line in (b).

Enrichment of Cr, Ni, Si, and Mo was observed adjacent to the outer oxide layer. In fact, formation of such phases occurred within the Si-enriched region after S-CO₂ exposure, which is indicated by chemical composition fluctuations in the EDS line scan result shown in Figure 6c. It seems that these phases are same as those formed after Si coating and heat treatment. Their formation would be related

to chemical composition changes that occurred with Si and Cr content decrease in the surface-modified region due to oxide formation.

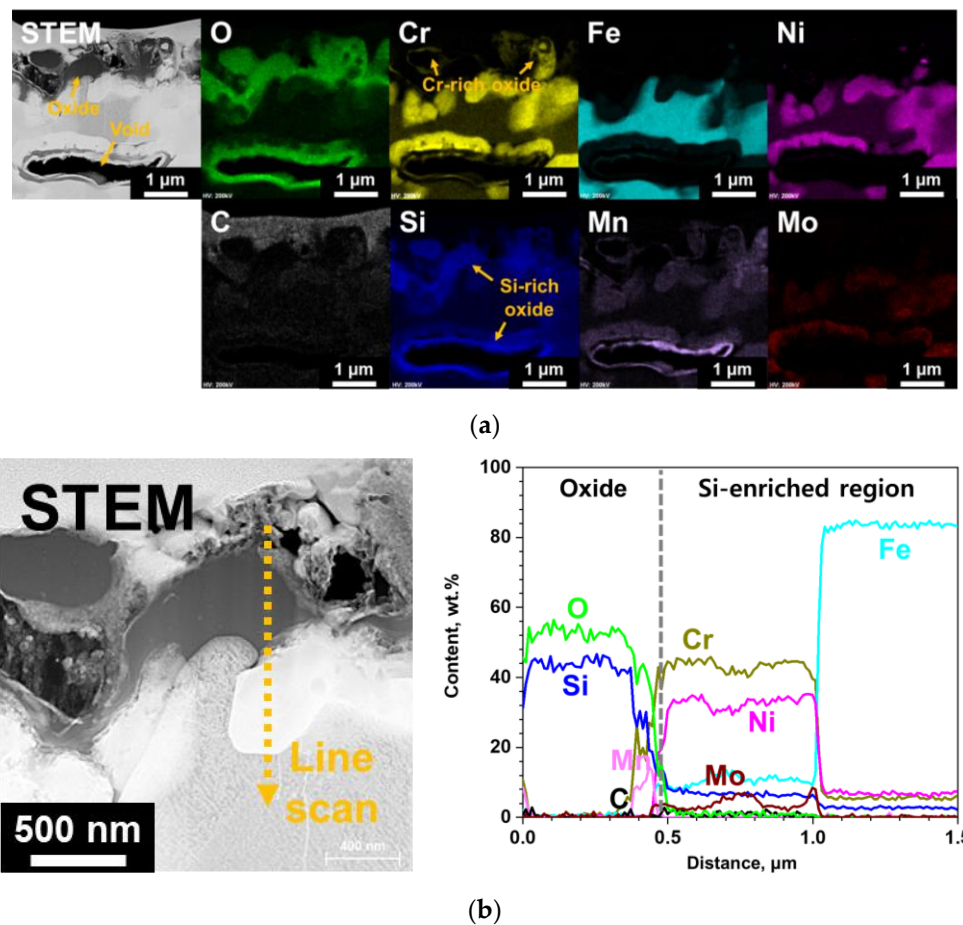


Figure 7. TEM analyses results of the surface-modified SS 316LN after exposure to S-CO₂ at 650 °C (20 MPa) for 500 h. (a) Scanning transmission electron microscope (STEM) image with EDS mapping images and (b) result of EDS line scan along the dotted line in magnified STEM micrograph on the left-hand side.

3.4. Characterization of Oxides Formed in High Temperature Steam

Figure 8 shows the surface SEM micrograph of the as-received SS 316LN corroded in steam. The surface is mostly covered in large Fe-rich oxides, while some thin continuous Cr-rich oxide regions can also be found. This is quite similar to that observed for the as-received SS 316LN after S-CO₂ exposure, only the extent of oxidation is greater in steam. Indeed, cross-sectional BSE micrograph shows that the Fe-rich oxides have thicknesses of greater than 40 μm (Figure 8b). In addition, similar to that found in S-CO₂-exposed as-received specimen, the oxides are composed of outer Fe-rich oxide and inner Fe- and Cr-rich spinel (Figure 8c).

The results of SEM analysis on the surface-modified SS 316LN after steam exposure are shown in Figure 9. A continuous oxide layer without any signs of spallation can be seen on the surface (Figure 9a). In case of its cross-section, the oxide is about 15 μm in thickness (Figure 9b), which is significantly smaller than that formed on steam-exposed as-received specimen (Figure 8b). Meanwhile, as shown in EDS line scan result in Figure 10b, the oxide layer has a complex structure composed of various oxides. Still, from TEM analyses result on the oxide shown in Figure 10, existence of Si-rich oxide can be seen below the outermost Fe-rich oxide. These observations are similar to those made in a previous work by Bolivar et al. in which 9Cr ferritic-martensitic steel (FMS) coated by Si using

chemical vapor deposition (CVD) was subjected to steam oxidation at 650 °C for up to 3000 h [16]. Si coating significantly reduced mass gains compared to those of the as-received alloy, which was ascribed to the formation of Si-rich oxide layer between the outer Fe-rich oxide and inner Fe- and Cr-rich spinel. Furthermore, Ishitsuka et al. reported similar corrosion behaviors and oxide structures for Si-containing FMS after high temperature steam exposure, and found the Si-rich oxides to be amorphous [17]. TEM analyses performed on the Si-rich oxide formed on the surface-modified alloys after steam corrosion in this study also revealed it to be amorphous (not shown).

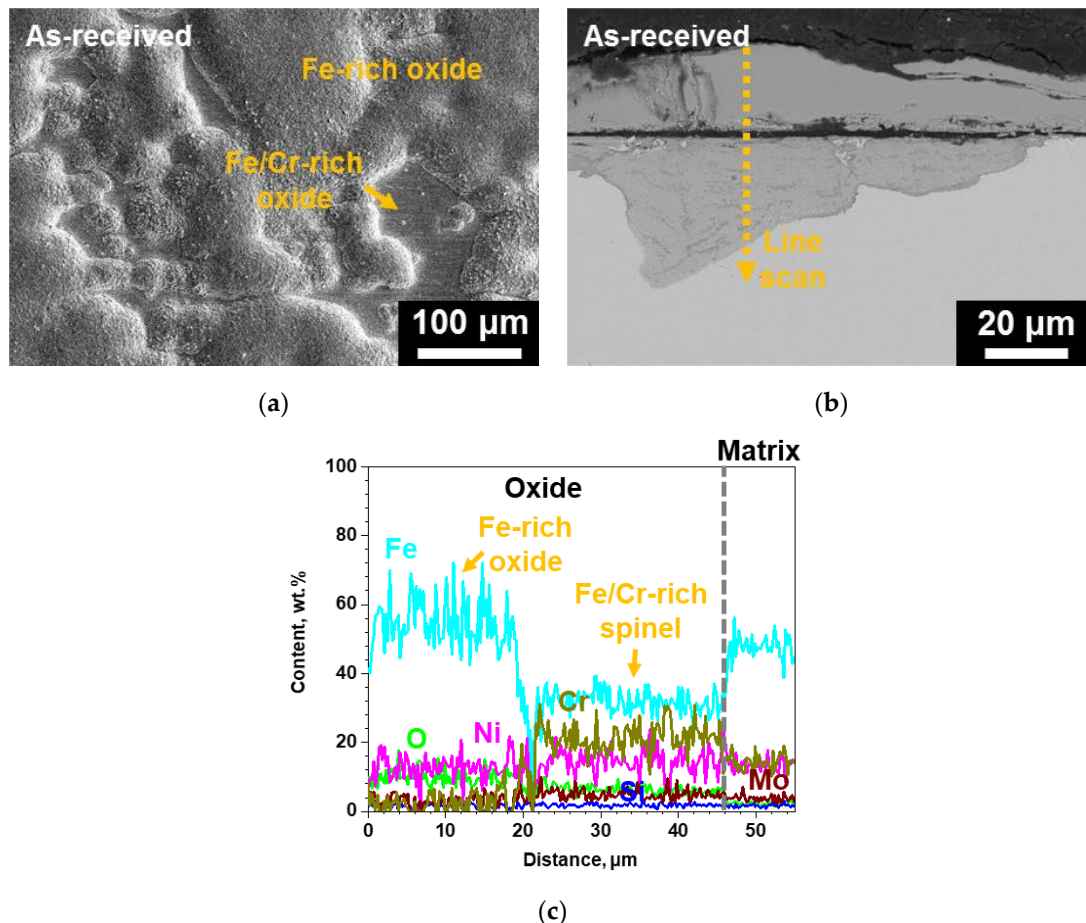


Figure 8. (a) Surface SEM, (b) cross-sectional BSE micrograph of the as-received SS 316LN after exposure to steam at 650 °C (0.1 MPa) for 500 h, and (c) result of EDS line scan along the dotted line in (b).

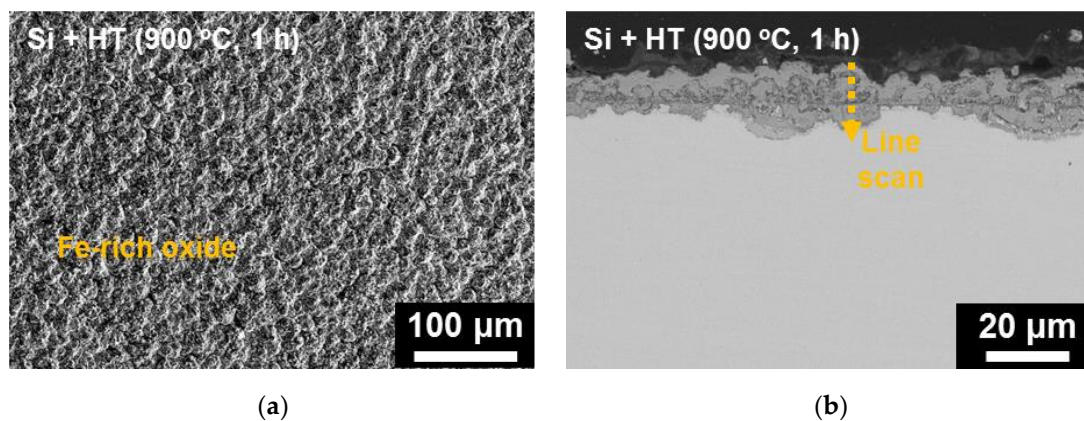


Figure 9. Cont.

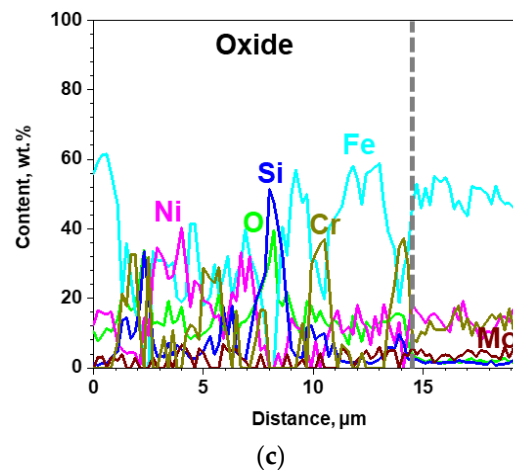


Figure 9. (a) Surface SEM, (b) cross-sectional BSE micrograph of the surface-modified SS 316LN after exposure to steam at 650 °C (0.1 MPa) for 500 h, and (c) result of EDS line scan along the dotted line in (b).

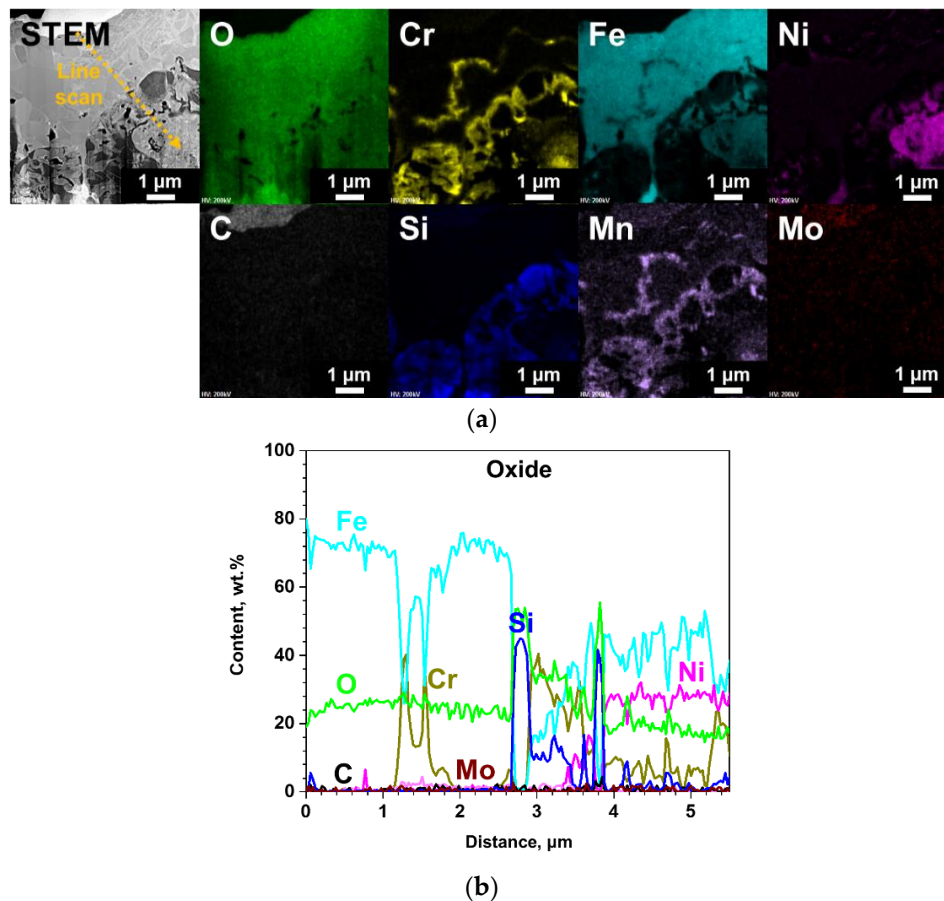


Figure 10. TEM analyses results of the surface-modified SS 316LN after exposure to steam at 650 °C (0.1 MPa) for 500 h; (a) STEM image with EDS mapping images, and (b) result of EDS line scan along the dotted line in STEM micrograph in (a).

Furthermore, results of XRD analysis conducted on the as-received and surface-modified SS 316LN after steam corrosion test at 650 °C (0.1 MPa) for 500 h are shown in Figure 11. For the as-received specimen, peaks of Fe_2O_3 and Fe_3O_4 oxides were detected, while only Fe_2O_3 was detected for the surface-modified SS 316LN. Matrix peaks were not detected for both specimens, because of the

thickness of the oxides as seen in the cross-sectional BSE images. In previous works in which duplex oxide were formed on FMS after high temperature exposure, it was reported that the outer Fe-rich oxide was composed of outermost Fe_2O_3 layer under which Fe_3O_4 was formed [18,19]. It was proposed that Fe_3O_4 initially forms, when the supply of Fe to the oxidation front is sufficiently high. With continued growth and increase in thickness of Fe_3O_4 layer on FMS, outward diffusion of Fe cations from the matrix to the oxidation front decreases. Consequently, at some point during oxidation, Fe_2O_3 forms at the outermost region above Fe_3O_4 , as Fe_2O_3 is stable at higher oxygen activities compared to Fe_3O_4 [20]. This mechanism could be applied to the as-received SS 316LN oxidized in steam in this study, in view of its oxide products (Fe_2O_3 and Fe_3O_4) and structure (duplex oxide). On the other hand, the absence of Fe_3O_4 for the surface-modified specimen would be due to the formation of Si-rich oxides, which hampered outward diffusion of Fe ions. Therefore, it is quite apparent that Si-rich oxides formed on the surface-modified alloys contributed to slower corrosion kinetics in high temperature steam environment.

Meanwhile, it should be noted that thickness of the oxide layer formed on the surface-modified alloy in steam environment is about 15 μm (Figure 9), which is greater than the thickness of the Si-enriched region of 9 μm (Figure 2). This implies that the oxide growth in steam extended to below the entire surface-modified region. Voids found in the Si-enriched region for surface-modified alloy (Figure 2) could not be observed along the entire sample. In addition, the Si content below the oxide layer of the surface-modified alloy in steam is about 1 wt.%, which is similar content as that detected in the matrix of the as-received SS 316LN. Despite the Si depletion after steam oxidation, surface Si-enrichment was effective in enhancement of oxidation resistance. However, sub-oxide depletion of an element participating in oxidation is a concern in oxide stability and there is a need for longer exposure tests in order to further validate the effectiveness of the surface-modification.

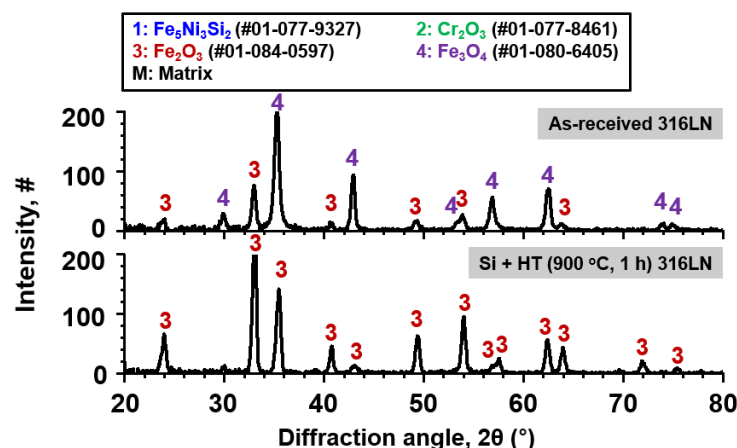


Figure 11. Result of XRD analysis conducted on the as-received and surface-modified SS 316LN after exposure to steam at 650 °C (0.1 MPa) for 500 h.

4. Conclusions

Si diffusion coating was formed on SS 316LN by Si deposition and subsequent heat treatment at 900 °C for 1 h. Si deposition and heat treatment on SS 316LN resulted in the formation of $\text{Fe}_5\text{Ni}_3\text{Si}_2$ phase as a surface layer, containing about 10 wt.% Si. Voids and Mo-enrichment was observed adjacent to the coating/matrix interface. The surface-modified alloy was exposed to high temperature S- CO_2 (650 °C, 20 MPa) and steam (650 °C, 0.1 MPa) for 500 h for the evaluation of its corrosion behavior. Steam exposure resulted in significantly greater oxidation for both the as-received and surface-modified alloys than after S- CO_2 exposure, despite higher pressure of S- CO_2 environment. Surface-modified SS 316LN exhibited enhanced corrosion behavior compared to that of the as-received alloy in both environments, by formation of relatively thin and continuous oxide layer. In S- CO_2 , Si-rich oxides

formed on the surface-modified specimen prevented oxide spallation and Fe-rich oxide formation, while in steam, oxidation rates were notably slow compared to the as-received alloy.

Author Contributions: Conceptualization, data curation, investigation, writing—original draft preparation S.H.K.; investigation, formal analysis, C.K.; investigation, J.-H.C.; conceptualization, supervision, writing—Review and editing, C.J. All authors have read and agreed to the published version of the manuscript.

Funding: This study was supported by two Nuclear R&D programs (Nos. 2020M2A8A4025453 and 2020M2A8A4023937) of MSIT/NRF of Korea. Financial support for three of the authors is provided by the BK-Plus Program of the MSIT/NRF of Korea.

Conflicts of Interest: The authors declare no conflict of interest.

References

1. Anderson, M.; Nellis, G.; Corradini, M. *Materials, Turbomachinery and Heat Exchangers for Supercritical CO₂ Systems*; NEUP Final Report (09-778); NEUP: Washington, DC, USA, 2012.
2. Tan, L.; Pint, B.A. *High-Temperature Steam Oxidation Testing of Select Advanced Replacement Alloys for Potential Core Internals*; ORNL Technical Report (ORNL/TM-2017/228); ORNL: Oak Ridge, TN, USA, 2017.
3. Nguyen, T.D.; Zhang, J.; Young, D.J. Effects of silicon and water vapour on corrosion of Fe-20Cr and Fe-20Cr-20Ni alloys in CO₂ at 650 °C. *Oxid. Met.* **2017**, *87*, 541–573. [[CrossRef](#)]
4. Moon, J.; Kim, S.; Park, W.D.; Kim, T.Y.; McAlpine, S.W.; Short, M.P.; Kim, J.H.; Bahn, C.B. Initial oxidation behavior of Fe-Cr-Si alloys in 1200 °C steam. *J. Nucl. Mater.* **2019**, *513*, 297–308. [[CrossRef](#)]
5. Kim, S.H.; Subramanian, G.O.; Kim, C.; Jang, C.; Park, K.M. Surface modification of austenitic stainless steel for corrosion resistance in high temperature supercritical-carbon dioxide environment. *Surf. Coat. Technol.* **2018**, *349*, 415–425. [[CrossRef](#)]
6. Lee, H.J.; Kim, H.; Kim, S.H.; Jang, C. Corrosion and carburization behavior of chromia-forming heat resistant alloys in high-temperature supercritical-carbon dioxide environment. *Corros. Sci.* **2015**, *99*, 227–239. [[CrossRef](#)]
7. Kim, D.; Kim, D.; Lee, H.J.; Jang, C.; Yoon, D.J. Corrosion characteristics of Ni-base superalloys in high temperature steam with and without hydrogen. *J. Nucl. Mater.* **2013**, *441*, 612–622. [[CrossRef](#)]
8. Zhang, W.-W.; Xu, H.-H.; Liang, J.-L.; Xiong, W.; Du, Y. Phase equilibria of the Fe-Ni-Si system at 850 °C. *J. Alloy. Compd.* **2009**, *481*, 509–514. [[CrossRef](#)]
9. Perez, F.J.; Hierro, M.P.; Carpintero, C.; Pedraza, F.; Gomez, C. Silicon deposition on AISI 304 stainless steel by CVD in fluidized bed reactors: Analysis of silicide formation and adhesion of coatings. *Surf. Coat. Technol.* **2001**, *40*, 93–98. [[CrossRef](#)]
10. Chen, H.; Kim, S.H.; Kim, C.; Chen, J.; Jang, C. Corrosion behaviors of four stainless steels with similar chromium content in supercritical carbon dioxide environment at 650 °C. *Corros. Sci.* **2019**, *156*, 16–31. [[CrossRef](#)]
11. Lee, H.J.; Subramanian, G.O.; Kim, S.H.; Jang, C. Effect of pressure on the corrosion and carburization behavior of chromia-forming heat-resistant alloys in high-temperature carbon dioxide environments. *Corros. Sci.* **2016**, *111*, 649–658. [[CrossRef](#)]
12. Wright, I.G.; Dooley, R.B. A review of the oxidation behavior of structural alloys in steam. *Int. Mater. Rev.* **2010**, *55*, 129–167. [[CrossRef](#)]
13. Stott, F.H.; Wood, G.C.; Stringer, J. The influence of alloying elements on the development and maintenance of protective scales. *Oxid. Met.* **1995**, *44*, 113–145. [[CrossRef](#)]
14. Bennett, M.J.; Desport, J.A.; Labun, P.A. Analytical electron microscopy of a selective oxide scale formed on 20%Cr-25%Ni-Nb stainless steel. *Oxid. Met.* **1984**, *22*, 291–306. [[CrossRef](#)]
15. Li, B.; Gleeson, B. Effects of silicon on the oxidation behavior of Ni-base chromia-forming alloys. *Oxid. Met.* **2006**, *65*, 101–122. [[CrossRef](#)]
16. Bolivar, F.J.; Sanchez, L.; Hierro, M.P.; Perez, F.J. Evaluation of Si coating on ferritic steels by CVD-FBR technology in steam oxidation. *Defect Diffus. Forum* **2009**, *289*, 413–420. [[CrossRef](#)]
17. Ishitsuka, T.; Inoue, Y.; Ogawa, H. Effect of silicon on the steam oxidation resistance of a 9%Cr heat resistant steel. *Oxid. Met.* **2004**, *61*, 125–142. [[CrossRef](#)]

18. Zurek, J.; Michalik, M.; Schmitz, F.; Kern, T.-U.; Singheiser, L.; Quadakkers, W.J. The effect of water-vapor content and gas flow rate on the oxidation mechanism of a 10%Cr-ferritic steel in Ar-H₂O mixtures. *Oxid. Met.* **2005**, *65*, 401–422. [[CrossRef](#)]
19. Rouillard, F.; Furukawa, T. Corrosion of 9–12Cr ferritic-martensitic steels in high-temperature CO₂. *Corros. Sci.* **2016**, *105*, 120–132. [[CrossRef](#)]
20. Dudziak, T. Steam oxidation of Fe-based materials. In *High Temperature Corrosion*; Ahmad, Z., Ed.; IntechOpen: London, UK, 2016; pp. 15–38.



© 2020 by the authors. Licensee MDPI, Basel, Switzerland. This article is an open access article distributed under the terms and conditions of the Creative Commons Attribution (CC BY) license (<http://creativecommons.org/licenses/by/4.0/>).